Versatile Double-Templating Synthesis Route to Silica Monoliths Exhibiting a Multimodal Hierarchical Porosity

Jan-Henrik Smått,[†] Stephan Schunk,[‡] and Mika Lindén*,[†]

Department of Physical Chemistry, Abo Akademi University, Porthansgatan 3-5, FIN-20500 Turku, Finland, and hte Aktiengesellschaft, Kurpfalzring 104, D-69123 Heidelberg, Germany

Received October 28, 2002. Revised Manuscript Received February 7, 2003

Monolithic silica exhibiting a trimodal, hierarchical pore structure has successfully been prepared via sol−gel-processing. Monolithic bodies with interconnected macropores in the micrometer range are a result of controlled phase separation and gelation kinetics, whereas textural mesopores in the 10−20 nm range originate from voids between particles. Furthermore, the particles exhibit internal mesoporosity with pore diameters in the 2−4 nm range originating from supramolecular templating by the surfactant. Poly(ethylene glycol) has been used together with alkylammonium surfactants to control the particle aggregation and internal structure, respectively. The present work sheds light on the mechanism of formation of the complex framework architectures and the application potential of the material.

1. Introduction

The synthesis of porous silica and other oxides has recently attracted immense interest. The use of supramolecular arrays of surfactants[1,2] or amphiphilic block copolymers[33] as structure-directing agents for the inorganic framework enables the synthesis of mesoscopically ordered materials exhibiting a narrow pore size distribution after removal of the organic portion. Other recent approaches utilize latex spheres,[4−9] (micro)emulsion droplets,[10−13] and macromolecules[14] for the generation of porosity. Furthermore, recent progress in the field of sol−gel chemistry enables macroscopic shape control to be achieved in parallel, and porous oxides have been prepared in the form of films, fibers, and monoliths. This is a necessary step toward expanding the application window of these materials beyond the scope of their use as sorbents, support materials, or the like in the direction of applications in the life science area. For many applications, such as chromatography, separation of large molecules, or drug release, to name a few, materials with both small and large pores arranged in a hierarchical structure-in-structure fashion are desirable. Such structures provide a high surface area and also minimize the pressure drop over the material. Additional surface functionalization of the siliceous materials can provide value in such applications as well.

Materials exhibiting micro/macroporosity and meso/macroporosity have been synthesized by the combination of two or more pore-building processes, zeolitic nanoparticles,[15−17] or supramolecularly templated inorganic aggregates[5,18,19] in combination with colloidal particles. Gel casting has also successfully been used to create hierarchical zeolitic[20] or mesoporous[21] structures with controlled shapes. Silica spheres have also been successfully transformed into zeolithic monoliths containing interconnected macropores.[22] Furthermore,

* To whom correspondence should be addressed. E-mail: mlinden@abo.fi.
† Abo Akademi University.
‡ hte Aktiengesellschaft.

(1) Kresge, C. T.; Leonowicz, M. E.; Roth, W. J.; Vartuli, J. C. *Nature* **1992**, *359*, 710.
(2) Beck, J. S.; Vartuli, J. C.; Roth, W. J.; Leonowicz, M. E.; Kresge, C. T.; Schmitt, K. D.; Chu, C. T.-W.; Olson, D. H.; Sheppard, E. W.; McCullen, S. B.; Higgins, J. B.; Schlenker, J. L. *J. Am. Chem. Soc.* **1992**, *114*, 10834.
(3) Krämer, E.; Förster, S.; Göltner, C.; Antonietti, M. *Langmuir* **1998**, *14*, 2027.
(4) Holland, B. T.; Blanford, C. F.; Stein, A. *Science* **1998**, *281*, 538.
(5) Antonietti, M.; Berton, B.; Göltner, C.; Hentze, H. *Adv. Mater.* **1998**, *10*, 154.
(6) Park, S. H.; Qin, D.; Xia, Y. *Adv. Mater.* **1998**, *10*, 1045.
(7) Wijnhoven, J. E. G.; Vos, W. L. *Science* **1998**, *281*, 802.
(8) Yang, P.; Deng, T.; Zhao, D.; Feng, P.; Pine, D. J.; Chmelka, B. F.; Stucky, G. D. *Science* **1998**, *282*, 2244.
(9) Velev, O. D.; Jede, T. A.; Lobo, R. F.; Lenhoff, A. M. *Chem. Mater.* **1998**, *10*, 3597.
(10) Schacht, S.; Huo, Q.; Voigt-Martin, I. G.; Stucky, G. D.; Schüth, F. *Science* **1996**, *273*, 768.
(11) Imhof, A.; Pine, D. J. *Nature* **1997**, *389*, 948.
(12) Schmidt-Winkel, P.; Lukens, W. W.; Zhao, D.; Yang, P.; Chmelka, B. F.; Stucky, G. D. *J. Am. Chem. Soc.* **1999**, *121*, 254.
(13) Feng, P.; Bu, X.; Stucky, G. D.; Pine D. J. *J. Am. Chem. Soc.* **2000**, *122*, 944.
(14) Davis, S. A.; Burkett, S. L.; Mendelson, N. H.; Mann, S. *Nature* **1997**, *385*, 420.
(15) Holland, B. T.; Abrams, L.; Stein, A. *J. Am. Chem. Soc.* **1999**, *121*, 4308.
(16) Huang, L.; Wang, Z.; Sun, J.; Miao, L.; Li, Q.; Yan, Y.; Zhao, D. *J. Am. Chem. Soc.* **2000**, *122*, 3530.
(17) Rhodes, K. H.; Davis, S. A.; Caruso, F.; Zhang, B.; Mann, S. *Chem. Mater.* **2000**, *12*, 2832.
(18) Yin, J. S.; Wang, Z. L. *Appl. Phys. Lett.* **1999**, *74*, 2629.
(19) Lebeau, B.; Fowler, C. E.; Mann, S.; Farcet, C.; Charleux, B.; Sanchez, C. *J. Mater. Chem.* **2000**, *10*, 2105.
(20) Wang, H.; Huang, L.; Wang, Z.; Mitra, A.; Yan, Y. *Chem. Commun.* **2001**, 1364.
(21) Liang, C.; Dai, S.; Guiochon, G. *Chem. Commun.* **2002**, 2680.
(22) Dong, A.; Wang, Y.; Tang, Y.; Zhang, Y.; Reu, N.; Gao, Z. *Adv. Mater.* **2002**, *14*, 1506.

10.1021/cm0213422 CCC: $25.00
Published on Web 05/13/2003

mesoporous/macroporous silica has been prepared by coating bacterial threads with silicate−surfactant mesophases.[14] However, chemical means of inducing phase and domain separation during synthesis has also successfully been applied in the synthesis of siliceous materials exhibiting a hierarchical porosity.[23,24] In a series of papers,[24] Nakanishi and co-workers used a wide variety of water-soluble polymers, such as poly(ethylene oxide) (PEO), to control the phase separation/gelation kinetics in the preparation of monolithic silica of virtually any shape exhibiting both interconnected macropores and textural mesoporosity. The macropore diameter can easily be controlled by adjusting the polymer concentration, since the timing of the phase separation relative to the sol−gel transition determines the macropore size. The walls in this macroporous structure consist of aggregates of silica nanoparticles giving rise to textural mesoporosity in the walls with pore sizes in the 10−20 nm range and a high specific surface area. The mesopore sizes can be controlled nearly independently of the macropore sizes through postsynthesis treatment in ammonia solution. Because the solubility of silica is dependent on both pH and temperature, an increase in one or the other will enhance Ostwald ripening of the silica matrix, leading to an increase in the mesopore diameter. These macroporous/mesoporous materials have already been applied in high-performance liquid chromatography (HPLC) and as catalyst supports, both of which require large pores for liquid or gas transportation through the material coupled with high surface areas.[25,26] Recently, the same group used block copolymers of the $(EO)_x-(PO)_y-(EO)_x$ type instead of PEO in a similar synthesis, and monoliths with a similar bimodal pore size distribution could be prepared. In this case, the mesopores were in the 2−3 nm range and were suggested to be structure directed by supramolecular aggregates of the amphiphilic block copolymer, similar to what has been observed for SBA-15 type materials. However, it is also possible to synthesize highly porous silicas using cationic surfactants as structure-directing agents under acidic conditions.[27] These materials, which are obtained in the form of powders, named SBA-3, also have pore sizes in the range of 2−3 nm and exhibit a regular, two-dimensional hexagonal arrangement of pores. The materials closely resemble the M41S type of materials introduced by scientists from the Mobile Oil Corporation in 1992, with the exception that the pore walls of the SBA-3 materials are microporous. The motivation for the present work is to try to combine two synthesis approaches in the synthesis of monolithic silica exhibiting multimodal porosity, the first one being polymer-controlled phase separation of silica particles during gelation in combination with a second approach using surfactants that can act as a supramolecular templates.

Table 1. Typical Starting Compositions for the Different Series Presented in This Paper

	molar ratios					
series[a]	H_2O	HNO_3	TEOS	PEG	C_nTAB	n
P-*	14.69	0.25	1.00	0.54−0.64	0.00	−
S-**	14.69	0.25	1.00	0.54	0.00−0.09	16
PS-$^+$	14.69	0.25	1.00	0.58−0.17	0.00−0.24	16
CL-$^{++}$	14.69	0.25	1.00	0.40	0.105	14−18

[a] P denotes polymer; S, surfactant; and CL, chain length. The series are indexed as follows: * = 54−64, ** = 00−90, $^+$ = 58−17/000−240, $^{++}$ = 14−18. The values given for the PEG were calculated on the basis of the monomeric units.

2. Experimental Section

2.1. Materials. Tetraethoxysilane (TEOS, Fluka) was used as the silica source, while poly(ethylene glycol) (PEG) with an average molecular weight of 35 000 g/mol (Merck) was the phase-separation-inducing agent. Cetyltrimethylammonium bromides with different hydrocarbon chain lengths were employed to produce mesopores in the 2−4 nm range. $C_{14}TAB$ and $C_{18}TAB$ were purchased from Fluka and $C_{16}TAB$ from Aldrich. Nitric acid (65%, Merck) was used as the catalyst for the hydrolysis and condensation of TEOS. Ammonia (33%, J. T. Baker) was used in posttreatments of the monoliths. All chemicals were used without further purification.

2.2. Sample Preparation. The silica monoliths were prepared by adding TEOS to a mixture of PEG(35 000) dissolved in an aqueous nitric acid solution. The sol was subsequently stirred at room temperature until a clear solution was obtained. At this stage, CTAB was added to the sol, and stirring was continued until the surfactant was completely dissolved (the starting compositions are listed in Table 1). The sols were left to gel at 40 °C ($t_{gel} \approx 6-10$ h) and subsequently aged for at least 48 h at 40 °C. Solvent exchange was performed to increase the degree of condensation, and thus the stability, of the silica gels.[28] An efficient procedure for obtaining large textural pores was to keep the monoliths in a 1 M NH_4OH solution for 9 h at 90 °C (this procedure was applied to all samples). The volume of the solvent exchange solution was 10 times the volume of the monoliths. The monoliths were then acidified with a 0.1 M HNO_3 solution and washed with ethanol (25 wt %). The monoliths were dried for 3 days at 60 °C in open beakers and then subsequently calcined at 550 °C for 5 h under air. The heating ramp was 1 K/min.

2.3. Structure Observation. The morphology of the calcined monoliths was investigated by scanning electron microscopy (LEO 1560) and transmission electron microscopy (Hitachi HF 2000). The transmission electron microscope was operated at 200 keV and equipped with a cold field emission source. Samples were mounted on carbon films that were fixed on copper grids. The size distributions of pores larger than 10 nm were measured by mercury porosimetry (AutoPore III, Micromeritics Co., Norcross, GA), and a contact angle of 130° was assumed in the pore size calculations. The pressure range varied between 690 Pa and 400 MPa. Pores smaller than 50 nm were measured by nitrogen sorption (ASAP 2010, Micromeritics Co., Norcross, GA) at 77 K. The desorption branch was used for pore size analysis.

3. Results

In the following discussion, the synthesis and characterization of porous, monolithic silica materials exhibiting a multimodal porosity is described. Because the procedure employed results in the formation of a silica gel, the size and shape of the monolith are determined by the size and shape of the vessel used. Typically, monolithic rods with diameters in the range of 4−8 mm

(23) Zhao, D.; Yang, P.; Chmelka, B. F.; Stucky, G. D. *Chem. Mater.* **1999**, *11*, 1174.
(24) Nakanishi, K. J. *Porous Mater.* **1997**, *4*, 67 and references therein.
(25) Minakuchi, H.; Nakanishi, K.; Soga, N.; Ishizuka, N.; Tanaka, N. *Anal. Chem.* **1996**, 68, 3498.
(26) Nakamura, N.; Takahashi, R.; Sato, S.; Sodesawa, T.; Yoshida, S. *Phys. Chem. Chem. Phys.* **2000**, *2*, 4983.
(27) Huo, Q.; Margolese, D. I.; Ciesla, U.; Demuth, D.; Feng, P.; Gier, T. E.; Sierger, P.; Firouzi, A.; Chmelka, B. F.; Schüth, F.; Stucky, G. D. *Chem. Mater.* **1994**, *6*, 1176.
(28) Ishizuka, N.; Minakuchi, H.; Nakanishi, K.; Soga, N.; Tanaka, N. *J. Chromatogr. A* **1998**, *797*, 133.

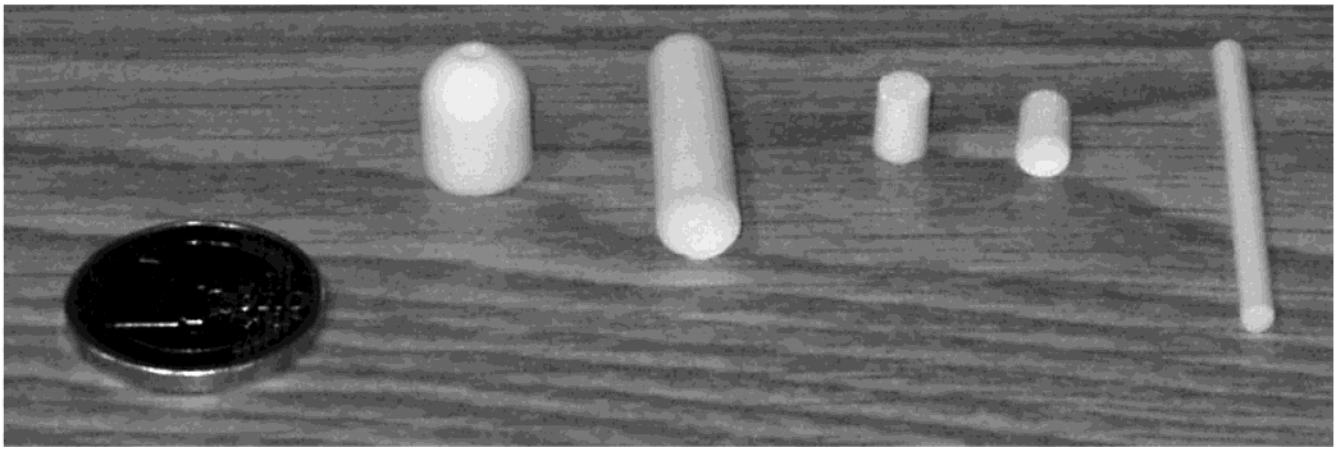

Figure 1. Photograph of monoliths of different shapes exhibiting multimodal hierarchical porosity. The diameter of the coin is 23 mm.

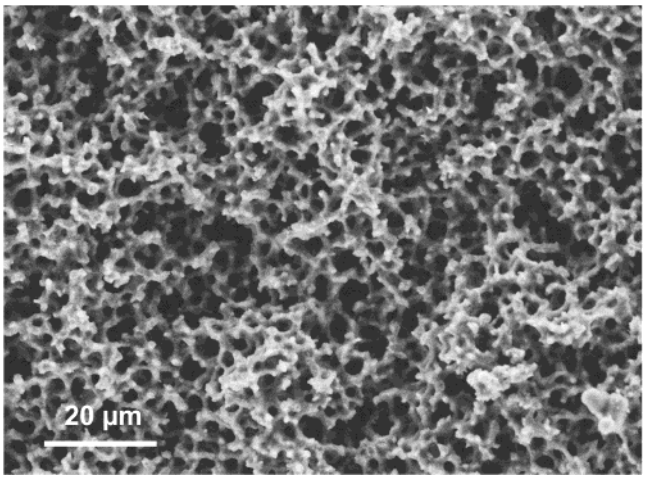

Figure 2. SEM image of a macroporous sample (P-62). Magnification = 1000×, scale bar = 20 μm.

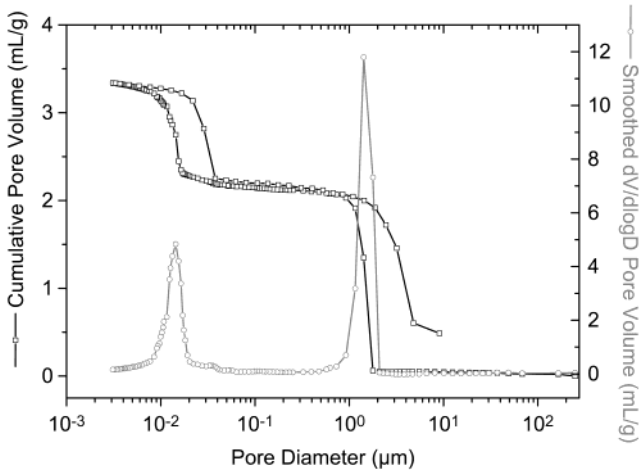

Figure 3. Pore size distribution of sample P-62 determined by mercury porosimetry. The open squares (□) denote the cumulative pore volume plot (intrusion and extrusion branch), while the open circles (○) denote the smoothed d*V*/(d log *D*) pore volume plot (intrusion branch).

and lengths of 1−4 cm were prepared, examples of which are shown in Figure 1. It is important to note that, during the processing of the materials, a shrinkage of the greenbody was observed that averaged 10−20% of the size of the gelled silica body. All compositions discussed below led to the formation of a macroporous, interconnected, open network of the type shown in Figure 2, with a narrow pore size distribution as can be seen in Figure 3. The macroporous nature of the monoliths is responsible for their white color.

Influence of the PEG(35 000)/TEOS Ratio. Nakanishi and co-workers have already established that there is a linear relationship between the logarithmic plot of the pore diameter versus the poly(ethylene oxide)/TEOS ratio in the compositional window that would lead to an interconnected macroporous structure in the monoliths. However, in their study, PEO with molecular weights of 20 000 and 50 000 were used. Therefore, it was important to determine the similar relation for the PEG(35 000) used in this study as a starting point. The macropore diameter, *D*, was determined by mercury porosimetry (intrusion) and confirmed by SEM. In Figure 4, the dependency of the macropore diameter of a sol with a $TEOS/HNO_3/H_2O$ molar composition of 1:0.25:14.69 on the PEG/TEOS molar ratio is shown. It is clear that the macropore diameter decreases with increasing PEG/TEOS ratio, as expected. A linear

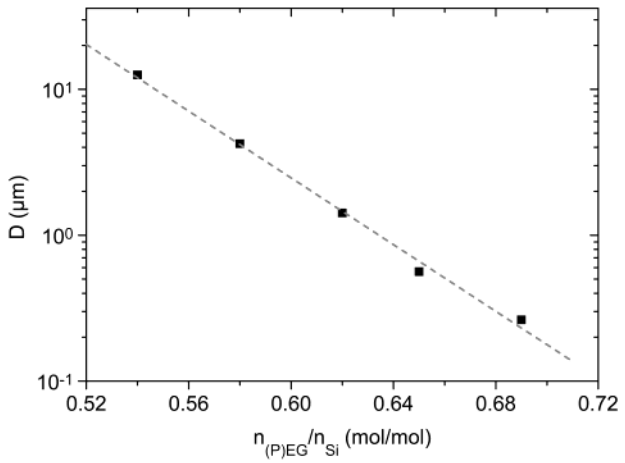

Figure 4. Evolution of the macropore diameter as a function of the PEG/Si ratio for series P.

relationship between log *D* and the PEG(35 000)/TEOS ratio was observed, with a slope being very similar to what previously was reported for PEO(20 000) and PEO(50 000). However, the absolute values that we observed are slightly lower than those reported by Nakanishi and co-workers, although they are still in acceptable ac-

Table 2. Effect on the Pore Size and the Pore Volume of Increasing the Amount of PEG (MW ≈ 35000 g/mol)[a]

sample	PEG/Si	d_{macro}[b] (μm)	d_{text}[b] (nm)	V_{macro}[c] (cm^3 g^{-1})	V_{text}[d] (cm^3 g^{-1})	V_{tot}[e] (cm^3 g^{-1})
P-54	0.54	12.56	14.4	1.71	1.34	3.06
P-58	0.58	4.24	14.4	1.96	1.04	3.00
P-62	0.62	1.42	14.4	2.17	1.17	3.34
P-65	0.65	0.563	15.6	2.20	1.16	3.36
P-69	0.69	0.263	16.2	2.43	1.02	3.45

[a] The TEOS/HNO_3/H_2O molar ratio was 1.00:0.25:14.69 in all cases. [b] Approximately determined from the mercury intrusion plot. [c] Determined from the cumulative mercury intrusion plot (d > 50 nm). [d] Determined from the cumulative mercury intrusion plot (d < 50 nm). [e] Does not contain any nitrogen physisorption contribution (V < 0.2 cm^3/g).

cordance. The minor difference might be due to differences in the PEG molecular weights, but it is more likely an effect of small differences in the temperature. The macropore volume increased with increasing PEG/TEOS ratio, as indicated in Table 2.[29]

Apart from the macropores, the monoliths also exhibit textural mesoporosity with a mean pore diameter of about 15 nm, as evidenced by mercury porosimetry, again in good agreement with that reported by Nakanishi and co-workers. The corresponding pore volumes and pore diameters for monoliths synthesized at various PEG/TEOS ratios are also listed in Table 2. As can be seen, the pore diameters and textural pore volumes are virtually independent of the PEG/TEOS ratio. The total pore volume exceeded 3 cm^3/g for all monoliths in this series and reached 3.45 cm^3/g for a monolith synthesized with a PEG/TEOS molar ratio of 0.69. The BET areas were 280 ± 20 m^2/g for all samples in this series.

Influence of the C_{16}TAB/TEOS Molar Ratio. To determine the influence of added C_{16}TAB on the macropore diameter, monoliths with a constant PEG/TEOS molar ratio of 0.54 were prepared at different CTAB/TEOS ratios. In all cases, an interconnected macropore structure was observed. The observed macropore diameters are listed in Table 3 and plotted as a function of the CTAB/TEOS molar ratio in Figure 5. It is clear that the macropore diameter first increases with increasing CTAB/TEOS ratio up to a CTAB/TEOS molar ratio of about 0.01 and then continuously decreases if more CTAB is added. Also, for these materials, a nearly linear dependence of the log D value on the C_{16}TAB/TEOS ratio was observed above the transition point. The macropore volume also increased with increasing amount of CTAB added, to reach a value of 2.8 cm^3/g. The textural mesopore diameter, on the other hand, remained almost constant at around 15 nm up to a CTAB/PEG ratio of 0.0435, after which it increased slightly to reach 18 nm at a CTAB/PEG ratio of 0.09. This increase was accompanied by a slight decrease in the textural mesopore volume (see Table 3) and a broadening of the textural mesopore size distribution. An SEM image of a monolith synthesized with low

(29) To exclude the possibility that compression effects during the mercury porosimetry measurements might have a profound influence on the results obtained, the total pore volumes of the monoliths were also determined gravimetrically according to the formula $V_{pore} = V_{monolith} - m_{monolith}\rho_{silica}$, where 2.19 cm^3/g was used as the density of amorphous silica. The values for the pore volume obtained from the combination of nitrogen physisorption and mercury porosimetry data and the pore volumes estimated from gravimetrical estimations were in mutual accordance within ±5% in all cases.

Table 3. Compositions and Mercury Porosimetry/Nitrogen Physisorption Data of Samples Containing C_{16}TAB[a]

sample	C_{16}-TAB/Si	d_{macro}[b] (μm)	d_{text}[b] (nm)	V_{macro}[c] (cm^3 g^{-1})	V_{text}[d] (cm^3 g^{-1})	V_{surf}[e] (cm^3 g^{-1})	V_{tot}[f] (cm^3 g^{-1})	BET area (m^2 g^{-1})
S-00	0.0000	13.9	14.5	1.73	1.40	0.18	3.30	276
S-04	0.0035	19.0	14.4	1.78	1.52	0.19	3.49	291
S-07	0.0070	12.4	14.9	2.07	1.44	0.20	3.72	306
S-11	0.0107	33.9	14.4	1.92	1.66	0.22	3.80	324
S-14	0.0143	26.7	14.4	2.29	1.49	0.24	4.02	358
S-18	0.0178	20.6	14.4	2.33	1.55	0.24	4.13	354
S-21	0.0214	12.4	15.0	2.25	1.39	0.25	3.89	370
S-29	0.0288	6.01	15.4	2.74	1.16	0.27	4.16	385
S-44	0.0435	2.64	14.4	2.90	1.13	0.34	4.38	484
S-59	0.0587	1.16	15.8	2.60	1.11	0.38	4.08	521
S-74	0.0741	0.925	17.3	2.76	1.08	0.45	4.30	620
S-90	0.0899	0.394	18.3	2.82	0.99	0.50	4.30	672
PS-34/137	0.1368	3.31	17.8	3.02	0.78	0.73	4.53	939
PS-26/187	0.1872	0.344	–	3.56	0.57	0.91	5.05	1106

[a] The TEOS/HNO_3/H_2O/PEG molar ratio was 1.00:0.25:14.69:0.54 for the samples in series S (S-00–S-90) and 1.00:0.25:14.69:0.34 and 1.00:0.25:14.69:0.26 for samples PS-34/137 and PS-26/187, respectively. [b] Approximately determined from the mercury intrusion plot. [c] Determined from the cumulative mercury intrusion plot (d > 50 nm). [d] Determined from the cumulative mercury intrusion plot (d < 50 nm). [e] Determined from the nitrogen adsorption isotherm (P/P_0 < 0.6). [f] Determined from both Hg porosimetry and N_2 adsorption.

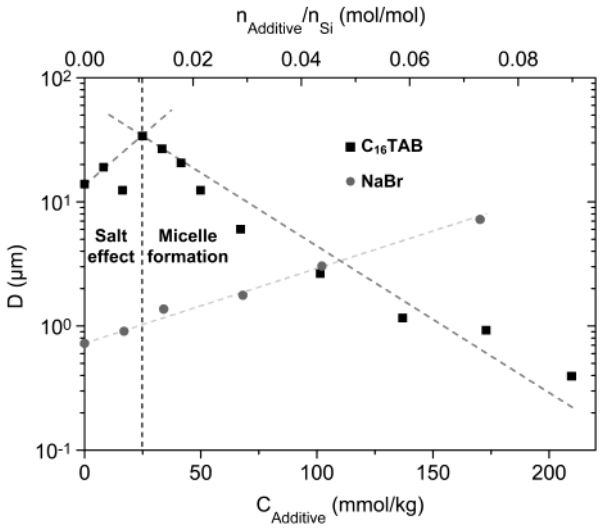

Figure 5. Slope of the plot of the CTABr/Si molar ratio versus ln D of the macropores. To demonstrate the salt effect, a similar series containing NaBr instead of CTABr was added. Note: The PEG/Si ratio was increased to 0.65 to avoid getting excessively large pores at high NaBr concentrations.

CTAB content is shown in Figure 6. It can be seen that the monolith is built up by aggregates of silica particles. Voids between these aggregates result in the observed textural porosity. More importantly, however, the formation of another population of mesopores with a narrow pore size distribution was observed at CTAB/PEG molar ratios exceeding 0.01, i.e., the region where the macropore size started to decrease. This is clearly seen in the N_2 sorption isotherms shown in Figure 7. A sharp increase in the adsorbed volume was observed at a relative pressure of 0.35, the sharpness of which was directly related to the amount of CTAB added. The corresponding BJH pore size diameter was 2.8–2.9 nm for all samples belonging to this group. The BET area also increased dramatically with increasing CTAB/

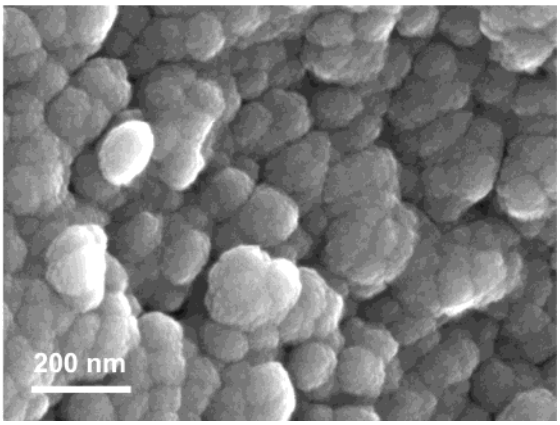

Figure 6. SEM image showing the textural porosity of sample S-11 (magnification = 100 000×, scale bar = 200 nm).

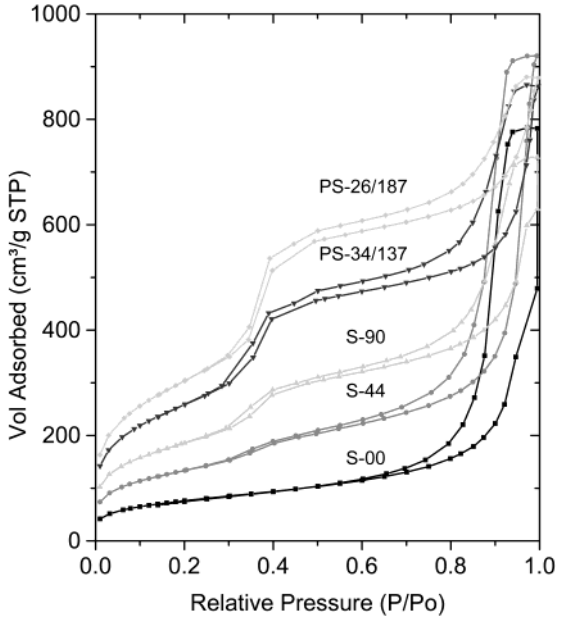

Figure 7. N_2 physisorption isotherms of samples S-00, S-44, S90, PS-34/137, and PS-26/187.

TEOS molar ratio, from 276 m^2/g at CTAB/TEOS = 0 to 672 m^2/g at CTAB/TEOS = 0.09. The total pore volume also increased in parallel to reach 4.3 cm^3/g.

Influence of the C_nTAB Chain Length. Some evidence for supramolecular templating of the mesopores can be gained from the characterization of samples prepared at constant PEG/TEOS and C_nTAB/TEOS ratios but with surfactants of different chain lengths. The N_2 sorption isotherms of monolithic silica prepared at a PEG/TEOS molar ratio of 0.40 and a C_nTAB/TEOS ratio of 0.105 (where n = 14, 16, and 18, or a 1:1 mixture of these) are shown in Figure 8. It is clearly seen that the relative pressure at which a pronounced increase in the adsorption is observed is shifted to higher values with increasing surfactant chain length, as previously observed for other materials exhibiting supramolecular templated mesopores.[2,27] From the $BJH_{desorption}$ plot (not shown), it could be determined that the pore size increases by about 0.32 nm with an increase in the chain length of the surfactant by two ethylene units. The total volume of adsorbed N_2 in this pressure range also increases with increasing chain length of the surfactant, reflecting the increase in the abundance of these mesopores. The BET areas, however, were similar, 755 ± 30 m^2/g, in all five cases, suggesting that the walls could contain additional microporosity, a common feature for surfactant-templated silica synthesized under acidic conditions.[30] A striking effect of the surfactant chain length is the decrease in the macropore size with increasing surfactant chain length, as reported in Table 4. Furthermore, the textural mesopore size also decreases with increasing surfactant chain length, as does the textural mesopore volume. However, the total pore volume of the monolith does not vary significantly (~4.5 cm^3g^{-1}) with increasing surfactant chain length.

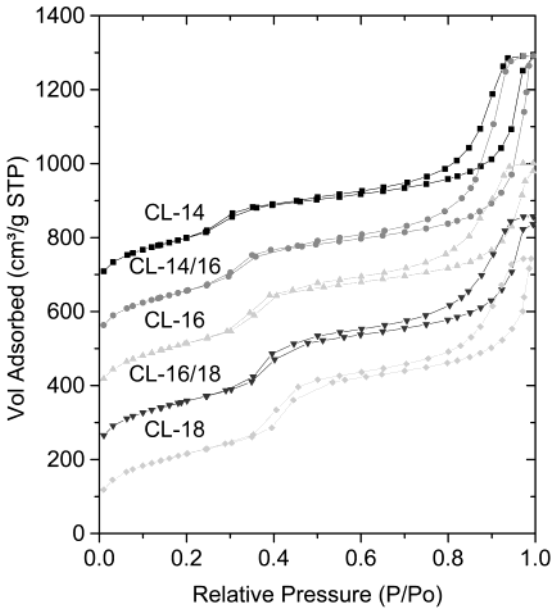

Figure 8. $C_{14}TABr-C_{18}TABr$. N_2 physisorption isotherms of silica monoliths synthesized in the presence of C_nTABr (n = 14, 16, 18) and 1:1 mixtures of these. The sorption isotherms are offset by 150 cm^3/g for clarity.

Simultaneous Variation of the PEG/TEOS and C_{16}TAB/TEOS Ratios. Because the macropore diameter decreases with increasing PEG/TEOS and C_nTAB/TEOS molar ratios in the concentration range where nontextural mesoporosity was observed, an attempt was made to simultaneously control the macroporosity and the mesoporosity by adjusting both parameters. To obtain larger macropores while still maintaining the surfactant-templated mesoporosity, the PEG/TEOS ratio was decreased with increasing CTAB/TEOS ratio. With this approach, the CTAB/TEOS ratio could be increased dramatically, resulting in a large fraction of nontextural mesopores with a $BJH_{desorption}$ pore diameter of 3 nm and a narrow pore size distribution (isotherms shown in Figure 7), mesopore volumes of up to 0.9 cm^3/g, and BET surface areas exceeding 1000 m^2/g, as also shown in Table 3 (samples PS-34/137 and PS-26/187). At the same time, the macropore size could be controlled independently by adjusting the PEG/TEOS ratio, which is evident from Table 2, when comparing samples with similar CTAB/TEOS molar ratios. The macropore size distribution remained narrow, and the porosity remained fully interconnected. The pore diameter of the textural mesopores increased slightly, and the pore size distribution broadened slightly. However, although the textural mesopore volume decreased to about 0.6 cm^3/g, the total pore volume remained high, exceeding 5 $cm^3/$

Table 4. Composition and Nitrogen Physisorption Data of Series CL[a]

sample	CTAB/Si	d_{macro}[b] (μm)	d_{surf}[c] (nm)	V_{macro}[d] ($cm^3\ g^{-1}$)	V_{text}[e] ($cm^3\ g^{-1}$)	V_{surf}[f] ($cm^3\ g^{-1}$)	V_{tot}[g] ($cm^3\ g^{-1}$)	BET area ($m^2\ g^{-1}$)
CL-14	0.105	24.1	2.55	2.64	1.15	0.49	4.28	723
CL-14/16	0.105[h]	18.8	2.74	2.94	1.09	0.55	4.58	749
CL-16	0.105	7.13	2.89	3.22	0.79	0.59	4.60	776
CL-16/18	0.105[h]	2.21	3.03	3.06	0.86	0.60	4.53	756
CL-18	0.105	0.708	3.21	3.12	0.72	0.65	4.49	782

[a] The TEOS/HNO_3/H_2O/PEG ratio for all samples was 1.00:0.25:14.69:0.40. [b] Approximately determined from the mercury intrusion plot. [c] Approximately determined from the $BJH_{desorption}$ plot. [d] Determined from the cumulative mercury intrusion plot (d > 50 nm). [e] Determined from the cumulative mercury intrusion plot (d < 50 nm). [f] Determined from the nitrogen adsorption isotherm (P/P_0 < 0.6). [g] Determined from both Hg porosimetry and N_2 adsorption. [h] 1:1 molar amount of C_{14}TAB/C_{16}TAB and C_{16}TAB/C_{18}TAB.

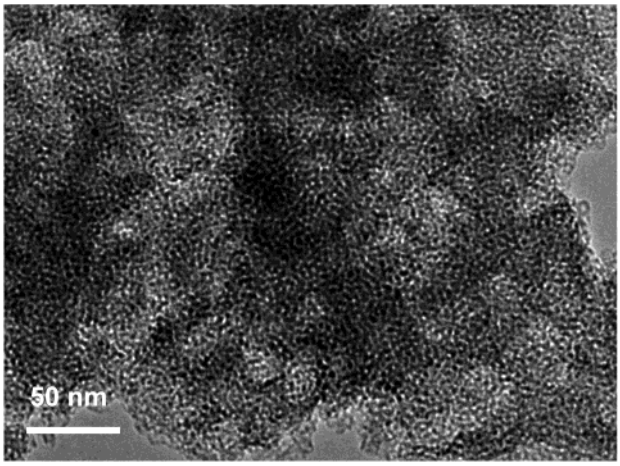

Figure 9. TEM micrograph of a porous monolith (PS-26/187) synthesized with C_{16}TABr and PEG(35 000). The scale bar corresponds to 50 nm.

g. The pore organization was also analyzed by TEM. As an example, a representative TEM image of a sample synthesized with a CTAB/TEOS ratio of 0.19 is shown in Figure 9. The narrow pore size distribution is evident here as well, as expected from the N_2 sorption measurements. However, the pore organization does not exhibit mesoscopic order, as observed for SBA-3 type materials, but rather, seems to be completely interconnected in a sponge-like manner and shows some similarity with the fractal macropore structure seen in the SEM image in Figure 2. No low-angle reflections can be observed in the XRD pattern for the presented materials (results not shown). This finding is opposite of what normally is observed for materials exhibiting supramolecularly templated mesopores, even for materials exhibiting a disordered, wormhole-like mesoporosity,[31] and again, it indicates that the mesopore walls could be microporous, which would result in a decrease in the scattering power.

4. Discussion

The results presented here clearly indicate that it is possible to synthesize silica monoliths with a trimodal pore size distribution by introducing a cationic surfactant to a sol−gel synthesis. Normally, such a synthetic effort would result in a gel exhibiting a bimodal pore size distribution in the absence of surfactant. With a careful adjustment of the relative ratios of the components, the macro- and mesoporosities can be controlled virtually independently of each other over several length scales. As discussed in a series of papers by Nakanishi and co-workers, the spinodal decomposition of gelling silica under acidic conditions can be controlled by the addition of PEG or other water-soluble, hydrogen-bonding polymers. The relative rates of gel formation and phase separation will determine the domain size of the final material. It is important to note that gelling silica in combination with such polymers can render materials of totally different character: mesoporosity, interconnected macroporosity, or macroscopic phase separation can all be observed, depending on the relative rates of gelation and phase separation.

At an r value of about 15 and at low pH, the silica nanoparticulates are small and initially clearly separated from each other, which makes solutions of such particles relatively stable. At the sol−gel transition, these systems tend form homogeneous monolithic gels. If PEG is added to the sol, the condensation process of the nanoparticulates is directed toward another mechanistic pathway. Because of the interaction of the polymer with the silica particles through hydrogen bonding[32] a phase separation into a polymer-rich phase and a silica-rich phase takes place. Silica, being the inorganic backbone, develops rigidity through intraparticle condensation and provides a framework of appreciable stability. A synthetic fine-tuning of these systems is possible and, in terms of compositional aspects, fairly simple: increasing the PEG/TEOS ratio will lead to bridging flocculation and eventually steric stabilization, with both effects being strongly dependent on the PEG molecular weight and the temperature.[33] By adjusting the PEG concentration moderately between these two particular regions, the onset of phase separation in relation to the sol−gel transition (and thus the domain size) can easily be controlled. This factor is the key element in accessing monolithic silica bodies with complex pore geometries with interconnected macropores in the range of 0.5−35 μm.

It has previously been established that the volume of the macropores can be adjusted simply by changing the water/silica ratio (r value) of the sol.[28] It should be kept in mind that these results were obtained under different conditions with regard to the sol−gel transition caused by the synthetic pathway. For the current work, however, the macropore volume varied between 1.7 and 3.5

(30) Göltner, C. G.; Smarsly, B.; Berton, B.; Antonietti, M. *Chem. Mater.* **2001**, *13*, 1617.
(31) Bagshaw, S. A.; Prouzet, E.; Pinnavaia, T. J. *Science* **1995**, *378*, 366.
(32) Rubio, J.; Kichener, J. A. *J. Colloid Interface Sci.* **1976**, *132*, 57.
(33) Ågren, P.; Rosenholm, J. B. *J. Colloid Interface Sci.* **1998**, *204*, 45.

cm^3/g, although the *r* value was kept fixed at 14.69. Here, the fluctuation in volume depends on the timing of the phase separation relative to the sol−gel transition. For an early phase separation, the amount of solvent that separates macroscopically before the silica structure "freezes" as a result of nanoparticle condensation is larger than that for a late phase separation. Because the volume of the macropore-forming agent (the solvent) is reduced inside the silica matrix, it is evident that the volume of the pores is also decreasing. Consequently, an increase in monolith size correlates well with an increase in macropore volume (see Table 2).

It is evident from the presented results that, above the CTAB/TEOS ratio at which the presence of "supramolecularly templated" mesopores were observed, an increase in either the PEG/TEOS ratio or the CTAB/TEOS ratio will result in a relative increase in the gelation rate compared to the rate of phase separation at a constant TEOS/H_2O molar ratio. In other words, in this concentration range, CTAB behaves similarly to PEG with regard to the condensation of the silica framework. On the other hand, at CTAB/TEOS ratios lower than the critical value, an increase in the surfactant concentration leads to an enlargement of the macropore diameter.

Our hypothesis was therefore that the different effects observed were coupled with the absence or presence of supramolecular surfactant aggregates in the sol. At surfactant concentrations lower than the critical concentration, the effect of CTAB would be similar to that of a simple nonaggregating salt, whereas the formation of mesopores with pore diameters in the range of 2−4 nm would be a result of the presence of CTAB micelles in solution. To gain support for our assumption, we carried out two types of experiments. The effect of added salt was studied for a series of monoliths that were synthesized in the presence of NaBr at a constant PEG/TEOS molar ratio of 0.65. A continuous increase in the macropore diameter was observed with increasing NaBr content, as shown in Figure 5, in a fashion similar to that observed in the dilute CTAB regime. The salt effects on the textural porosity were negligible. In a second set of experiments, the critical micelle concentration, cmc, of C_{16}TAB in an ethanol−water−nitric acid solution (molar ratio of 1:3.2:0.064) was determined by surface tension measurements at 40 °C. This ethanol/water/HNO_3 ratio was chosen to mimic the synthesis conditions of the sol−gel process: ethanol was added to the mixture according to the amount of ethanol released upon complete hydrolysis of TEOS. In Figure 10, the measured surface tension values are plotted against the C_{16}TAB concentration, and from this plot one can deduce a cmc value of about 26 mmol/kg. The cmc of C_{16}TAB in water is about 1 mmol/kg at 25 °C, and the much higher value observed in ethanol−water solution is directly correlated with the decrease in cohesive power of the solvent and is similar to what has been observed in water−methanol mixtures.[34] The cmc value determined for CTAB in ethanol−water solution is very close to the CTAB concentration (about 25 mmol/kg) at the critical point in Figure 5. Therefore, we can conclude that, at CTAB concentrations below the cmc,

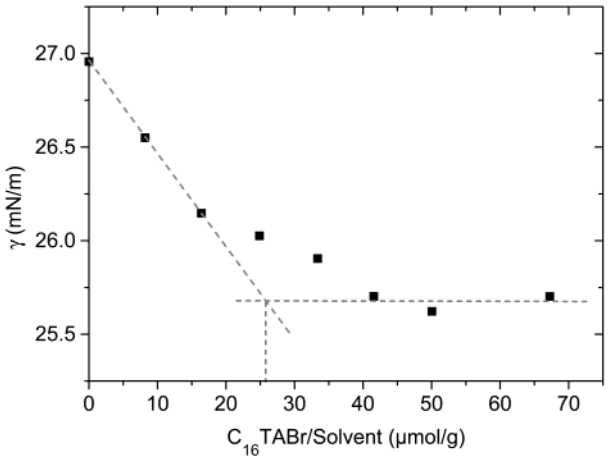

Figure 10. Determination of the critical micelle concentration (cmc) of a solution corresponding to the hydrolyzed and partly condensed sols of the samples in Table 3. The EtOH/H_2O/HNO_3 molar ratio of the solution is 1:3.2:0.064.

the effect of CTAB on the gelating silica is similar to that of a simple salt, whereas the presence of CTAB micelles is crucial for the formation of the supramolecularly templated mesopores in this system. The similarity in the influence of CTAB micelles and PEG on the aggregation of silica particles can be understood, as CTAB is able to chemically interact with silica and the micellar aggregates are also characterized by a high molecular weight. Furthermore, it is known that the interaction between PEG and cationic surfactants is weak,[35] this being the reason that the formation of PEG−CTAB micellar complexes will be of minor importance in this system. On the basis of these findings, we propose a simple reaction scheme in which the silica initially interacts with CTAB micelles, the aggregation of which is further controlled by the hydrogen-bonding PEG, as shown in Figure 11. More important support for the idea that a surfactant-induced supramolecular templating mechanism is relevant for mesopore formation is that the mesopore diameter is directly related to the alkyl chain length of the surfactant. Mesopore organization, however, cannot be observed, which might be related to the presence of PEG. TEM images show that the mesopores are completely disordered, as is also evidenced by the lack of low-angle reflections in the XRD pattern, which is distinctively different from the case for most other materials exhibiting surfactant-templated porosity. The TEM investigations also suggest that the mesopores are interconnected to a large degree. However, as already discussed, this effect can at least partially also be explained by the presence of micropores in the mesopore walls.

The findings discussed above illustrate that the silica nanoparticle/PEG interaction, leading to complex fractal pore architectures via phase separation, is strongly influenced by the presence of surfactants. The synthesis principle illustrated here demonstrates that it is essentially possible to control organization over several length scales simultaneously.

(34) Anderson, M. T.; Martin, J. E.; Odinek, J. G.; Newcomer, P. P. *Chem. Mater.* **1998**, *10*, 1490.
(35) Goddard, E. D. *Colloids Surf.* **1986**, *19*, 255.

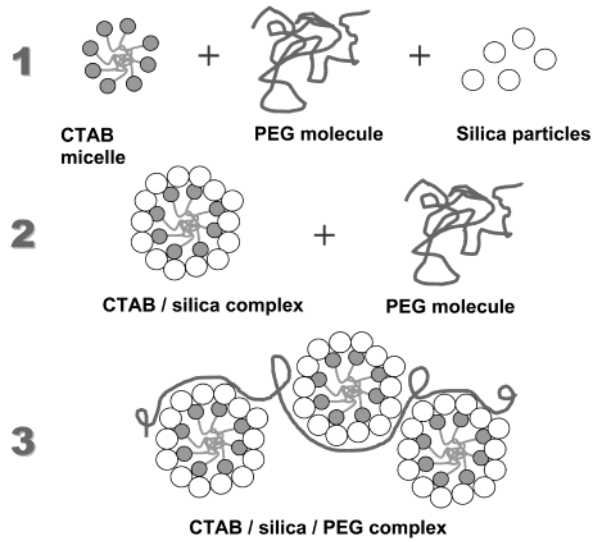

Figure 11. Schematic representation of the proposed steps involved in the formation of monolithic silica with multimodal porosity using a surfactant (CTAB) and a hydrogen-bonding homopolymer (PEG) as templates.

5. Conclusions

A combination of a water-soluble homopolymer and a surfactant, both being able to interact with silica nanoparticles, has been used to template monolithic silica exhibiting interconnected porosity on several length scales. The macropore diameter, which is mainly controlled via PEG/nanoparticle interactions, can be varied almost independently of the mesopore diameters through the incorporation of supramolecular CTAB aggregates by simultaneously varying the amounts of PEG and CTAB added. It is suggested that the presence of CTAB micelles is a prerequisite for the formation of surfactant-templated mesopores in this synthesis, whereas at surfactant concentrations below the cmc, the surfactant behaves as a simple salt. The material as such has a large range of possible applications, some inclassical fields such as catalysis and separation, with others being more advanced as support materials for drug release, bioactive membranes or biomimicking implant materials. The expansion of the synthetic principle to other inorganic materials such as salts and oxides and different surface-active components is underway.

Acknowledgment. The financial support of the HTE Company, Heidelberg, Germany, and The Finnish Academy of Sciences is gratefully acknowledged. The authors also thank Bernt Spliethoff, MPI, Mülheim/Ruhr, Germany, for carrying out the TEM work and Stefan Backlund for technical assistance.

CM0213422